

State of Health Estimation Based on OS-ELM for Lithium-ion Batteries

Yiduo Zhu^{1,2,3}, Fuwu Yan^{1,2}, Jianqiang Kang^{1,2}, Changqing Du^{1,2,*}

¹ Hubei Key Laboratory of Advanced Technology for Automotive Components, Wuhan University of Technology, Wuhan 430070, China

² Hubei Collaborative Innovation Center for Automotive Components Technology, Wuhan University of Technology, Wuhan 430070, China

³ Wuhan Technical College of Communications, Wuhan 430065, China

*E-mail: cq_du@whut.edu.cn

Received: 5 April 2017 / Accepted: 29 April 2017 / Published: 12 June 2017

An accurate state of health (SOH) estimation can facilitate the design of reliable battery systems and ensure reliability and safety during battery operation. An effective prediction algorithm is indispensable in performing an accurate SOH estimation. In this study, to solve the problem of obtaining battery capacity fading under the real vehicle state, the discharge time of equal voltage interval is used as the health indicator of the battery. The selection reason of the discharge voltage interval is explained from the aspects of battery mechanism and experimental data. To solve the problem of accuracy and large computation in SOH estimation, an online sequential extreme learning machine is used to predict SOH. The method demonstrates fast learning and generalization performance. The prediction error is less than 1.9%, which proves the accuracy of the method.

Keywords: State of health, Extreme learning machine, Health indicator, Lithium-ion battery

1. INTRODUCTION

Active energy supply is crucial in electric vehicles. For example, the working state of the battery is directly related to driving safety and operational reliability. To ensure that battery performance in electric vehicles is good and to extend battery life, the state of health (SOH) of the battery should be monitored timely and accurately. SOH estimation requires a practical algorithm. Therefore, relevant battery models and algorithms have been studied extensively.

Numerous studies have been conducted on the capacity fading modeling and algorithms of lithium-ion batteries to determine the correlation between capacity degradation and operating

conditions. Bole 1 presented a method of parameter adjustment in an electrochemical model of a lithium-ion battery. An unscented Kalman filtering algorithm was used to estimate model parameters according to collected battery current and voltage data. Liu 2 presented a Gaussian process model to obtain prognostics of battery health. The model provides variance around its mean predictions to describe associated uncertainty in the evaluation. Zhou 3 proposed a battery remaining useful life (RUL) prediction approach based on online support vector regression. Combined prediction with multi-models involving offline and online algorithms was realized to achieve improved prediction capacity. Saha 4 and Benjamin 5 proposed a particle filter algorithm to estimate SOH and predict RUL. The effect of the self-recharge phenomenon was determined and isolated simultaneously with the life cycle model. Pang 6 used time interval to equal discharge voltage difference as a battery health indicator (HI). The Gaussian process regression (GPR) algorithm was utilized for RUL estimation, and the confidence interval for the RUL value was provided. Jiang 7 selected the same HI. A relation model of extreme learning machine (ELM) based on the time interval to equal discharge voltage and capacity fading was built, and a prediction model of ELM based on the time interval to equal discharge voltage was proposed. Gering 8 presented a combination of sigmoidal rate expressions to interpret capacity loss. The combination covers main mechanisms that affect the loss of available lithium and active material. This method identifies reversible and irreversible capacity loss contributions and calculates molar-based terms for lithium and active sites. Gu 9 studied the internal kinetics of side reactions during the aging process and developed a crossover model that links the internal process with external phenomena. The author proved the operability and accuracy of the model for vehicle applications. Sankarasubramanian 10 built a capacity fading model for lithium-ion batteries that considered diffusion and kinetics. The Arrhenius equation was improved by considering the rate constant governing solid electrolyte interface (SEI) formation and solvent diffusivity. The relationship between capacity loss and SEI layer thickness was proven to vary linearly. Wu 11 presented an incremental analysis-based autoregressive exogenous modeling method and verified the findings in urban dynamic driving sequence profiles. The dynamic model can update parameters in real time. Zhou 12 used mean voltage fall off (MVF) as a novel HI for battery degradation modeling. The author predicted RUL by using an optimized relevance vector machine (RVM) given a linear correlation between MVF and capacity. Zhou 13 further proposed a combined model for RUL prognosis. Empirical model decomposition (EMD) and autoregressive integrated moving average (ARIMA) were considered in the combined model. Su 14 presented an orthogonal design of experiments to examine seven principal factors of battery fading. The deceleration factor for comparing fading capacity under different test conditions was used to improve the empirical aging model. Wu 15 utilized the feed-forward neural network (FFNN) and importance sampling (IS) to estimate the RUL of a lithium-ion battery online. FFNN was used to simulate the relationship between RUL and the charge curve, and IS was employed for FFNN input selection. Wang 16 assessed capacity degradation by adopting a state-space model for lithium-ion battery capacity. The model was solved by using a spherical cubature particle filter.

Based on electrochemical process, the battery life prediction model presents high accuracy and applicability. However, the model is complex and computationally expensive because it requires a comprehensive understanding of the internal process of the battery. Accurate parameters are also

difficult to achieve. The Arrhenius equation and its improved algorithm can help determine the general trend of battery decline. In the process of deriving battery decline, the coefficient is obtained from specific sample test data, and the analysis of the electrochemical mechanism is ignored. SOH estimation for a power battery based on the physical circuit model is mainly realized by online identification of the internal parameters of the power battery, such as voltage and internal resistance. However, these parameters are affected by the aging process of the battery, temperature, working current, operating point, measuring instruments, and other factors. These factors seriously affect the accuracy of SOH estimation.

Analysis of previous studies on SOH estimation indicates that neural network algorithms are seldom used to predict battery fading. One reason is the extensive algorithmic calculation required for online application. Another reason is the difficulty of acquiring large amounts of experiment data to train the network. Nevertheless, the neural network algorithm has significant advantages. The algorithm can compensate for the error of the model by increasing the sample data and learning frequency, thereby improving the accuracy of the estimation. Online sequential extreme learning machine (OS-ELM) demonstrates fast learning and generalization performance. It is suitable for regression, fitting problems, classification, pattern recognition, and other issues, so the range of its applications is wide.

In this study, a novel method is proposed to estimate the SOH of lithium-ion batteries through OS-ELM. ELM algorithm has been used in other studies without online function. The method of OS-ELM considerably reduces the computational cost of the neural network. Beside this, the discharge time of equal voltage interval is usually used as the HI of the battery. However, no other study has described how to select the voltage interval. In this study, according to fading mechanism of the battery, the center of voltage interval should be around the maximum peak of incremental capacity (IC) curve. This conclusion is verified by calculating correlation coefficient in this study. Compared with other relative studies, the results of SOH estimation with the novel method are more accurate. The proposed method is discussed in detail in Section 2. The contribution of this study is the establishment of a method with merits of high precision, simplicity, and rapid learning. This study also provides a theoretical basis for online SOH estimation.

2. THEORETICAL BACKGROUND

ELM is a type of single-hidden-layer feedforward neural network. The algorithm is characterized by the fact that the parameters of the hidden layer are randomly selected during the determination of network parameters. In the training process, the parameters need not be adjusted, and only the optimal solution can be obtained once the number of neurons in the hidden layer is selected. The output weight of the network is the least squares solution obtained by minimizing the squared loss function. Iterative steps are avoided in the process of determining the network parameters, so the adjustment time of the network parameters is reduced significantly. Compared with traditional training algorithms, the ELM algorithm possesses the advantages of fast learning and generalization performance [17,18]. The topological structure of the ELM network is shown in Fig. 1.

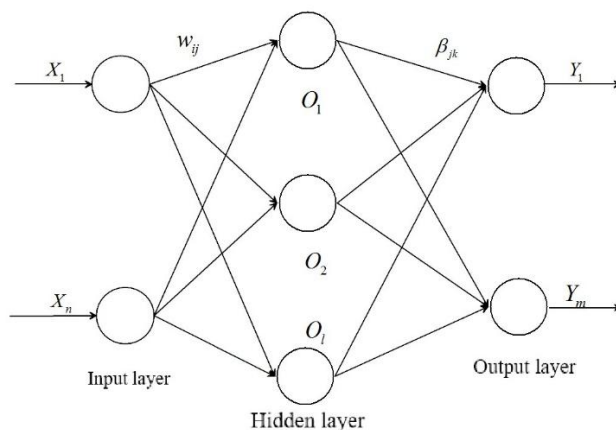


Figure 1. Topological structure of the ELM network

In Fig. 1, X_1, X_2, \dots, X_n are the input variants of ELM; Y_1, Y_2, \dots, Y_m are the outputs of ELM; and w_{ij} and β_{jk} are network weights.

Data collection is an online process in many practical cases. This condition means that not all sample data are acquired at one time but at a certain time. Hence, the data training process is highly complicated. The OS-ELM approach can effectively combine the training of old and new samples while avoiding the repetitive training of existing data [19,20].

The learning process of OS-ELM comprises two parts. The first part is the initial stage in which output weight β of the neural network is obtained from a small number of samples. The second part is the online learning stage in which β is updated by a single sample or several samples. The number and activated function of hidden layer neurons are l and g , respectively. In the initial stage, with a supposed number of N_0 , the training samples are denoted as (X_i, t_i) . $X_i = [x_{i1}, x_{i2}, \dots, x_{in}]^T$, $t_i = [t_{i1}, t_{i2}, \dots, t_{im}]^T$. Input weights w_i and input bias b_i ($i = 1, 2, \dots, N$) are initialized randomly. H_0 is the output matrix of the hidden layer.

$$H_0 = \begin{bmatrix} g(w_1, b_1, X_1) & \cdots & w_N, b_N, X_1 \\ \vdots & & \vdots \\ w_1, b_1, X_{N_0} & \cdots & w_N, b_N, X_{N_0} \end{bmatrix}_{N_0 \times N} \quad (1)$$

In the basic ELM algorithm, a $\beta^{(0)}$ must exist to endow $\|H_0\beta - T_0\|$ a minimal value. According to the calculation method of the generalized inverse matrix, $\beta^{(0)}$ is calculated as

$$\beta^{(0)} = P_0 H_0^T T_0, \quad (2)$$

where $P_0 = (H_0^T H_0)^{-1}$ and $T_0 = [t_1, t_2, \dots, t_{N_0}]^T$.

In the online learning stage, the output matrix of hidden layer H_i is calculated, followed by output weight β^i . If several samples or a single sample is input, β^i should be calculated with Eq. (3) or Eq. (4), respectively.

$$\begin{cases} P_{k+1} = P_k - P_k H_{k+1}^T (I + H_{k+1} P_k H_{k+1}^T)^{-1} H_{k+1} P_k \\ \beta^{(k+1)} = \beta^{(k)} + P_{k+1} H_{k+1}^T (T_{k+1} - H_{k+1} \beta^{(k)}) \end{cases} \quad (3)$$

$$\begin{cases} P_{k+1} = P_k - \frac{P_k h_{k+1} h_{k+1}^T P_k}{1 + h_{k+1}^T P_k h_{k+1}} \\ \beta^{(k+1)} = \beta^{(k)} + P_{k+1} h_{k+1} (t_{k+1}^T - h_{k+1}^T \beta^{(k)}) \end{cases} \quad (4)$$

SOH estimation based on ELM involves the following three steps.

Step 1: Modeling the discharge time prediction of equal voltage interval. The model is denoted as model 1, in which the discharge time sequence is used to establish training and testing datasets according to Eqs. (5) and (6), respectively. The first $m-1$ columns and the last column of the matrix are the input and output of the ELM network, respectively. In the test process, the first $m-1$ columns of the data test matrix are inputted to the ELM network, and the predicted discharge time is outputted from the networks. The predicted error is calculated by using predicted discharge time subtracting the last column of the data test matrix.

$$datatraining = \begin{bmatrix} t_1 & t_2 & \cdots & t_m \\ t_2 & t_3 & \cdots & t_{m+1} \\ \vdots & \vdots & \ddots & \vdots \\ t_{n-m+1} & t_{n-m+2} & \cdots & t_n \end{bmatrix} \quad (5)$$

$$datatest = \begin{bmatrix} t_{n-m+2} & t_{n-m+3} & \cdots & t_{n+1} \\ t_{n-m+3} & t_{n-m+4} & \cdots & t_{n+2} \\ \vdots & \vdots & \ddots & \vdots \\ t_{n+k-m+1} & t_{n+k-m+2} & \cdots & t_{n+k} \end{bmatrix} \quad (6)$$

Step 2: Modeling the relationship between discharge time of equal voltage interval and capacity. The model is denoted as model 2, in which the discharge time of equal voltage interval and capacity are the input and output of the ELM network, respectively. The experimental data in the next section are divided into training and test sets, which are used for ELM training and testing, respectively.

Step 3: SOH prediction. The predicted discharge time in model 1 is inputted to model 2, and the output of model 2 is the predicted capacity. The SOH value is calculated as follows:

$$SOH = \frac{C}{C_{init}}, \quad (7)$$

where C is the predicted or measured capacity of the battery and C_{init} is the initial capacity of the battery.

3. EXPERIMENT

Commercial Li(NiCoMn)O₂ cylindrical 18650 lithium-ion batteries were provided by Tianjin Lishen Battery Company. The PE material is Li(NiCoMn)O₂, and the NE material is graphite. The nominal capacity is 2.6 Ah. The charging and discharge cutoff voltages are 4.2 and 2.75 V, respectively. The multi-channel test equipment (model number CT4008) was provided by Tianjin NEWARE Electronics Company. The test temperature controlled by environmental chambers was

stable at 25 °C. The reference performance test (RPT), which includes capacity, hybrid pulse power characteristic, and IC tests, was used in accordance with the USABC test protocol **Error! Reference source not found.**

Several batteries were cycled in the state of charge (SOC) range of 0–0.3, 0.4–0.7, and 0.7–1 under discharge rates of 1C and 2C. The RPT test was performed after every 150 cycles. The experiments were stopped when 20% of the capacity of the batteries was consumed (from 2.6 Ah to 2.08 Ah). The experiments aimed to examine the effect of SOC cycle range on battery degradation and battery SOH prediction. Table 1 shows a matrix of the cycle aging test.

Table 1. Cycle aging test matrix

Battery	SOC range	Discharge rate	Cycle count
A	0–0.3	1C	4200
B	0–0.3	2C	4200
C	0.4–0.7	1C	4200
D	0.4–0.7	2C	4200
E	0.7–1	1C	4050
F	0.7–1	2C	2850

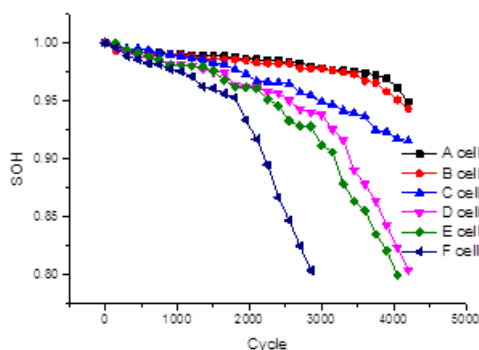


Figure 2. Comparison of battery fading among A to F batteries

Fig. 2 shows a comparison of the SOH of A to F batteries. Battery capacity was measured after every 150 cycles. The data on battery D were used as an example for discussion in the next section.

4. RESULTS AND DISCUSSION

4.1 Discharge voltage interval selection

Pang 6 selected the time of discharge voltage decline from 4.0 V to 3.6 V as a battery HI. Jiang 7 selected the time of discharge voltage decline from 3.8 V to 3.5 V as HI. However, why the voltage

interval was selected was not described in detail. In the current work, three voltage ranges, namely, 3.8 V to 3.6 V, 3.6 V to 3.4 V, and 3.8 V to 3.4 V, were selected as HI. With the increase in the number of cycles, battery capacity and the discharge time of the three voltage intervals decreased. In Fig. 3(a), the black square represents the variation in battery capacity with cycles. The red dots, green triangles, and blue inverted triangles represent the variation in the discharge times of the three voltage intervals with cycles. The variation trends of the four curves were similar. In Fig. 3(b), capacity and discharge time are normalized. The correlation between the normalized discharge time of the voltage range 3.6 V to 3.4 V curve and the normalized capacity curve are closer than the others. The correlation coefficient of the three discharge time curves and capacity curve were calculated according to the method described in Section 2. The results are shown in Table 2. The correlation coefficient between the normalized discharge time of the voltage range of 3.6 V to 3.4 V and normalized capacity was larger than the others. All capacity and discharge times were measured under current C/3.

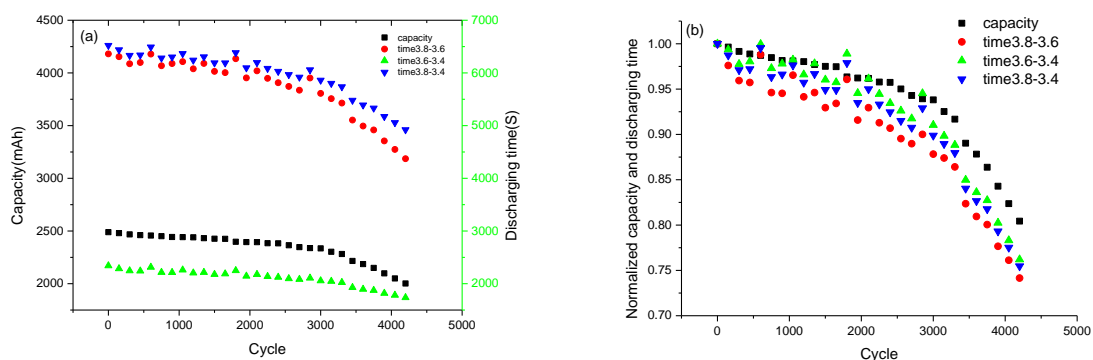


Figure 3. Capacity variation and discharge time variation of different voltage intervals: (a) before and (b) after normalization

Table 2. Correlation coefficient of the three discharge times and capacity

Discharge voltage interval	3.8 V to 3.6 V	3.6 V to- 3.4 V	3.8 V to 3.4 V
Correlation coefficient	0.9812	0.9861	0.9858

According to fading mechanism of the battery, for the IC curve ($-dQ/dV = f(V_{cell})$), every IC peak is a unique representation of a negative electrode (NE) reaction convoluting with a corresponding positive electrode (PE) reaction [22,23]. Fig. 4 shows the IC curve after different cycles at (a) C/3 and (b) C/25 discharge. In Fig. 4(b), the maximum peak intensity emerges at approximately 3.6 V, indicating that the greatest redox reaction occurs at this point. Empirically, the reaction at around 3.6 V is attributed to the characteristic of the chemical element Co [24,25], which suggests that some LiCoO₂ is present in the PE material. In Fig. 4(a), the maximum peak shows an early onset and a decrease in peak intensity when compared with the curve in Fig. 4(b). The polarization effect is inferred to be responsible for the phenomenon²⁶. Large polarization causes the maximum peak shift left at 3.5 V and the disappearance of several other peaks in the process of discharge. This condition

explains why the largest correlation coefficient occurred in the voltage interval of 3.6 V to 3.4 V. The voltage range can be adjusted according to actual needs.

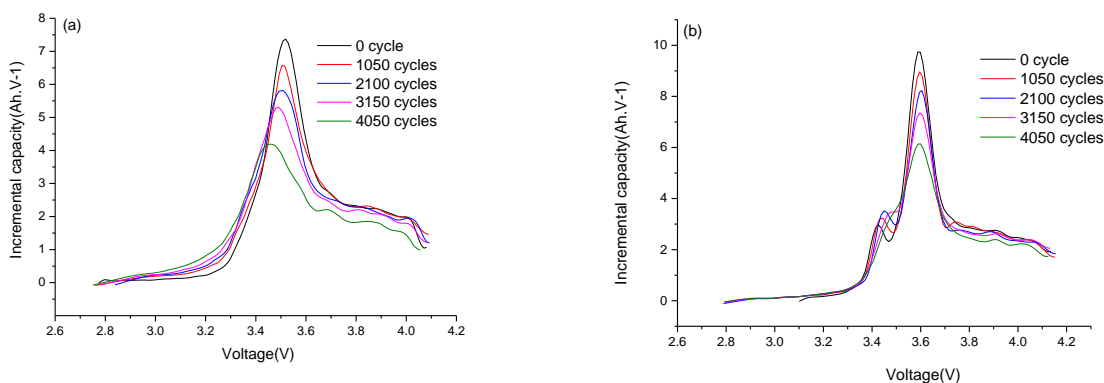


Figure 4. IC curve after different cycles at (a) C/3 and (b) C/25 discharge

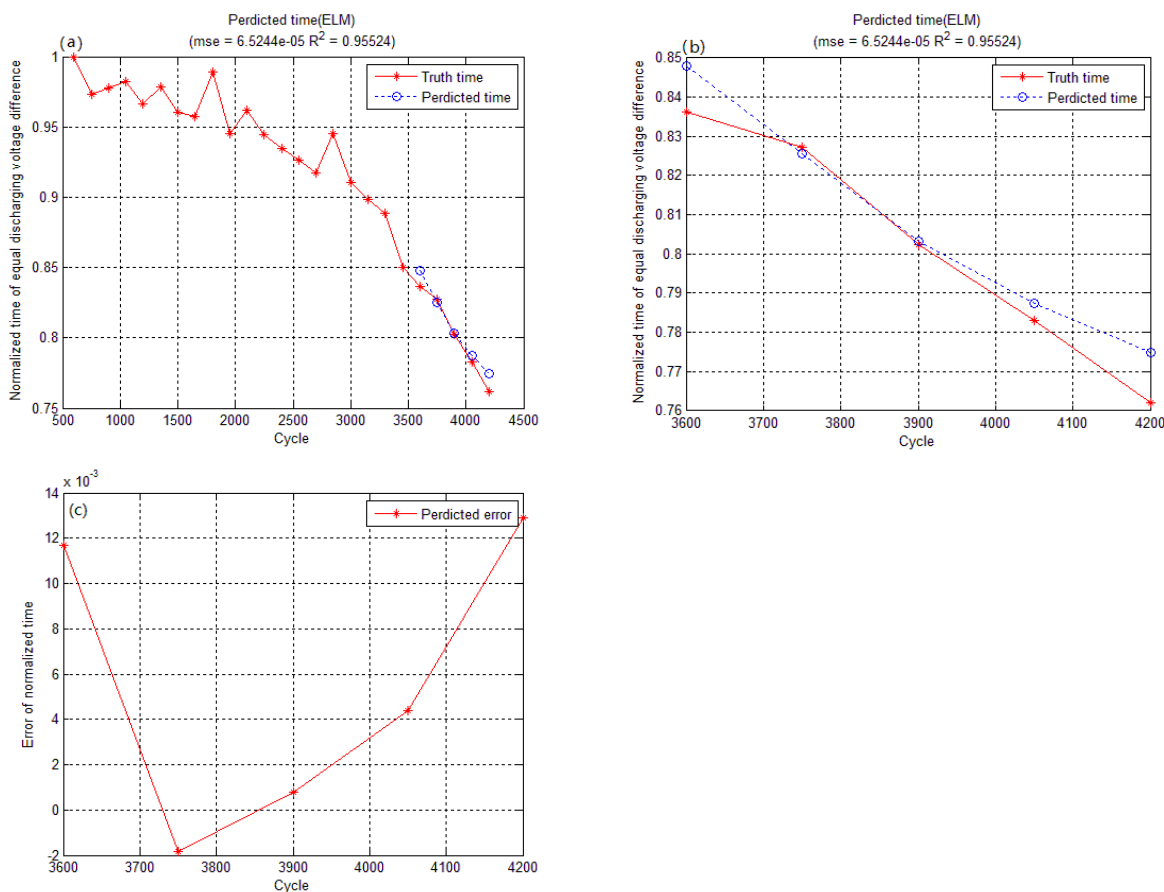
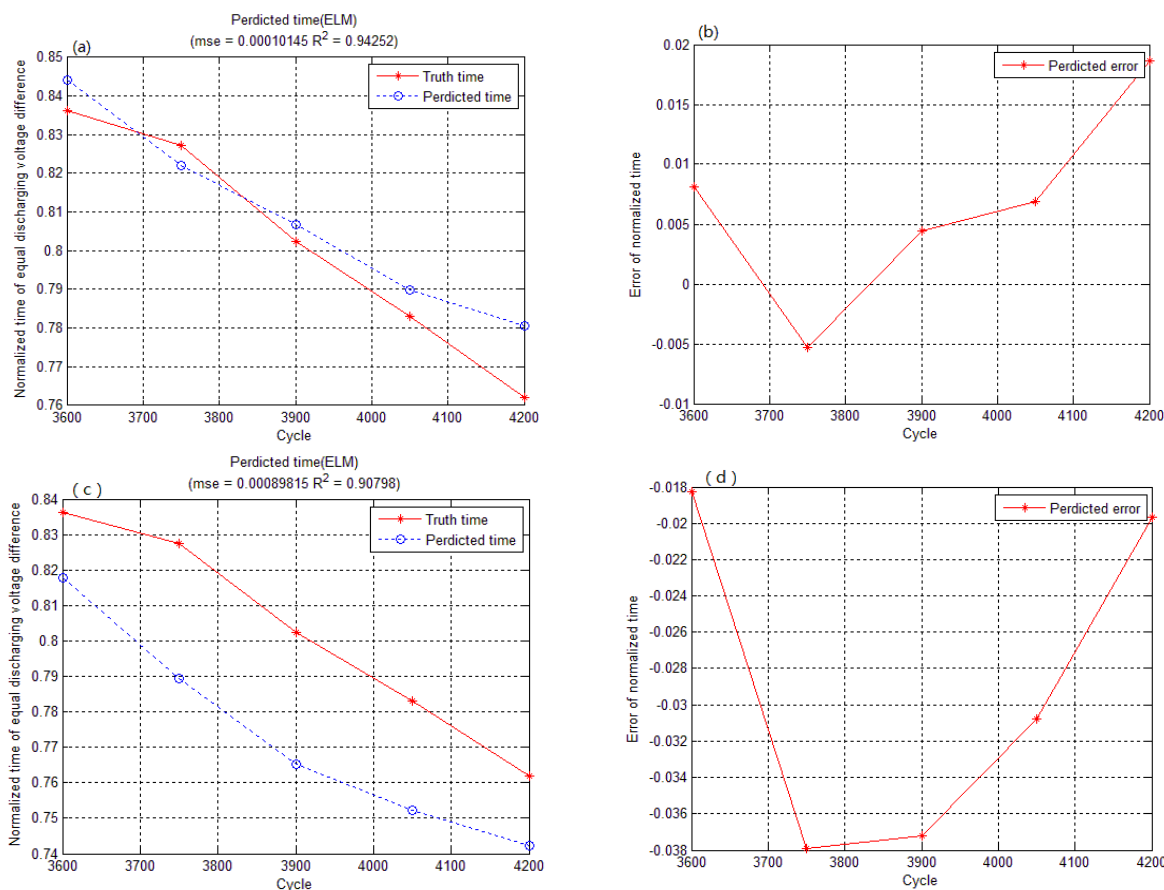


Figure 5. OS-ELM-predicted (a) (b) normalized time and (c) error of the equal discharge voltage difference

In model 1, the number of hidden neurons was 6. The discharge times before and after 3500 cycles were used to train and test the model, respectively. The predicted results and error of model 1

are shown in Fig. 6. In Fig. 6(a), the blue hollow circles represent the normalized predicted time of the equal discharge voltage difference calculated from model 1. The red asterisks represent the normalized true discharge time. The predicted time tracks the true time variation of the battery well. In Fig. 6(b), the detailed comparison of predicted and true times is amplified. In Fig. 6(c), the detailed comparison of predicted and true times is amplified. In Fig. 6(c), the red asterisks represent the predicted error obtained using the normalized predicted time subtracted by the normalized true time. All the errors are less than 0.013, which proves the accuracy of the OS-ELM algorithm.

The number of neurons in the hidden layer is crucial because its selection results directly affect network performance. If the number of neurons in the hidden layer is small, then the network cannot learn well. Increased time and cost will be required to train the network, and training accuracy may be insufficient. When the number of neurons in the hidden layer is within a reasonable range, increasing the number of neurons can improve the accuracy of network training and reduce the frequency of training. However, if the number of neurons is larger than the range, the time and cost of network training will increase. This effect can possibly cause other problems, such as falling into the local minima and reducing the learning speed. Thus far, no theory can explain how to determine the number of hidden layers in a network. Only by trying different numbers of neurons in the hidden layer can the most appropriate number be determined. As described above, the number of hidden neurons in this study was 6. Aside from this value, 4, 8, and 10 were tried. The predicted results and errors are shown in Fig. 6. Compared with those in Fig. 5, all the errors are larger than the error shown in Fig. 5(c). Therefore, the most appropriate hidden number of neurons is 6.



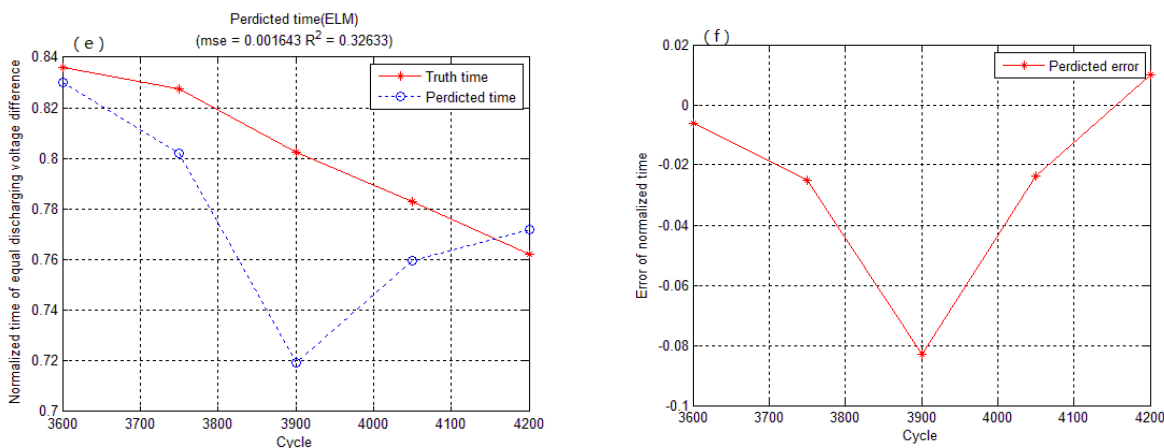


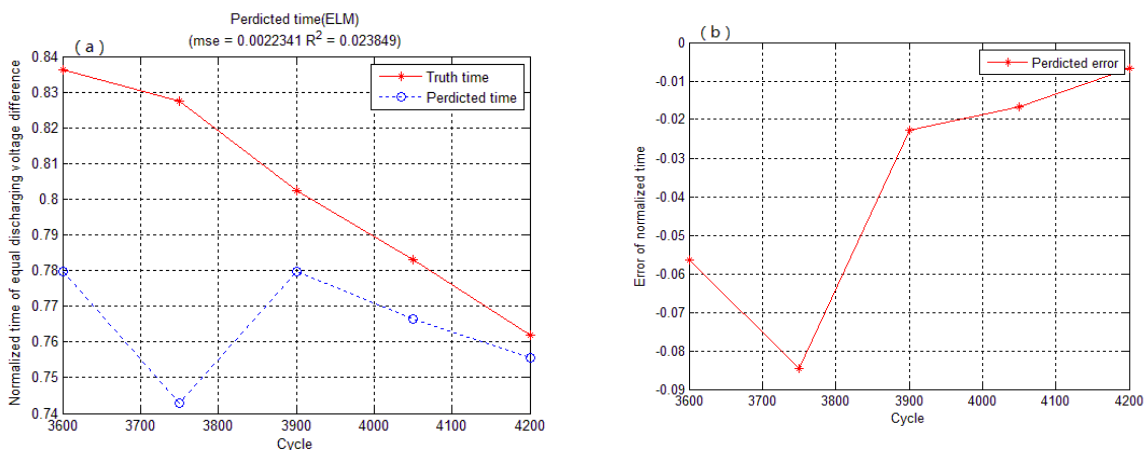
Figure 6. OS-ELM-predicted result and errors with (a)–(b) 4, (c)–(d) 8, and (e)–(f) 10 hidden layers neuron numbers

Table 3. Predicted errors and time cost of OS-ELM with different numbers of hidden layer neurons

Hidden neuron number	4	6	8	10
Max predicted error	0.018	0.013	0.038	0.082
MSE	1.015e-04	6.524e-05	8.982e-04	1.643e-03
Time cost (s)	0.5911	0.6722	0.6372	0.8894

Table 3 shows that the maximum predicted errors of 4, 6, 8, and 10 hidden layer neurons are 0.018, 0.013, 0.038, and 0.082, respectively. The predicted MSE of 4, 6, 8, and 10 hidden layer neurons are 1.015e-04, 6.524e-05, 8.982e-04, and 1.643e-03, respectively. The time cost differences among them are considerably small, which verifies that the most appropriate hidden neuron number is 6.

The activated function of hidden layer neurons is another important factor that affects ELM network performance. The activated function is selected as a sigmoid function by default. However, sin and hardlim functions can also be selected as the activated function of hidden layer neurons.



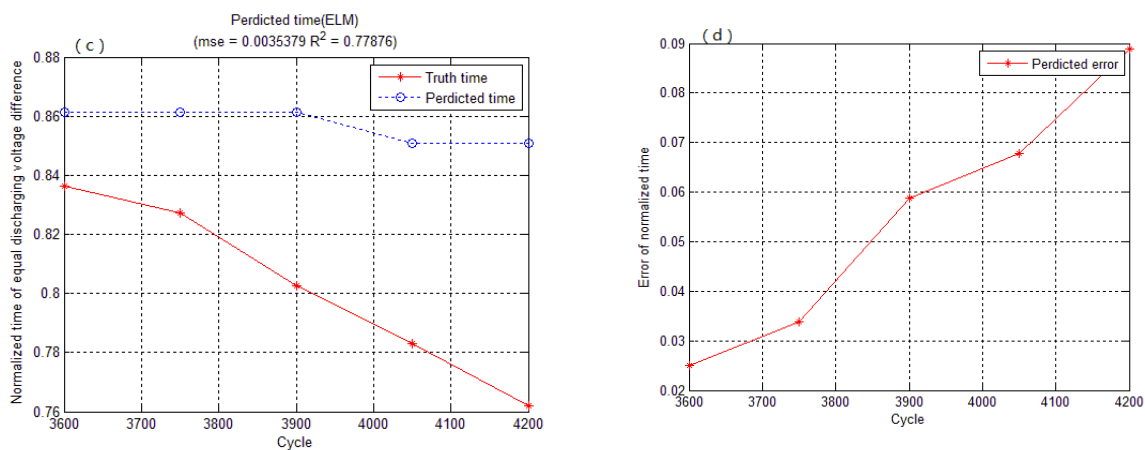


Figure 7. OS-ELM-predicted result and errors with different activation functions of hidden layer neurons: (a)–(b) sin function and (c)–(d) hardlim function

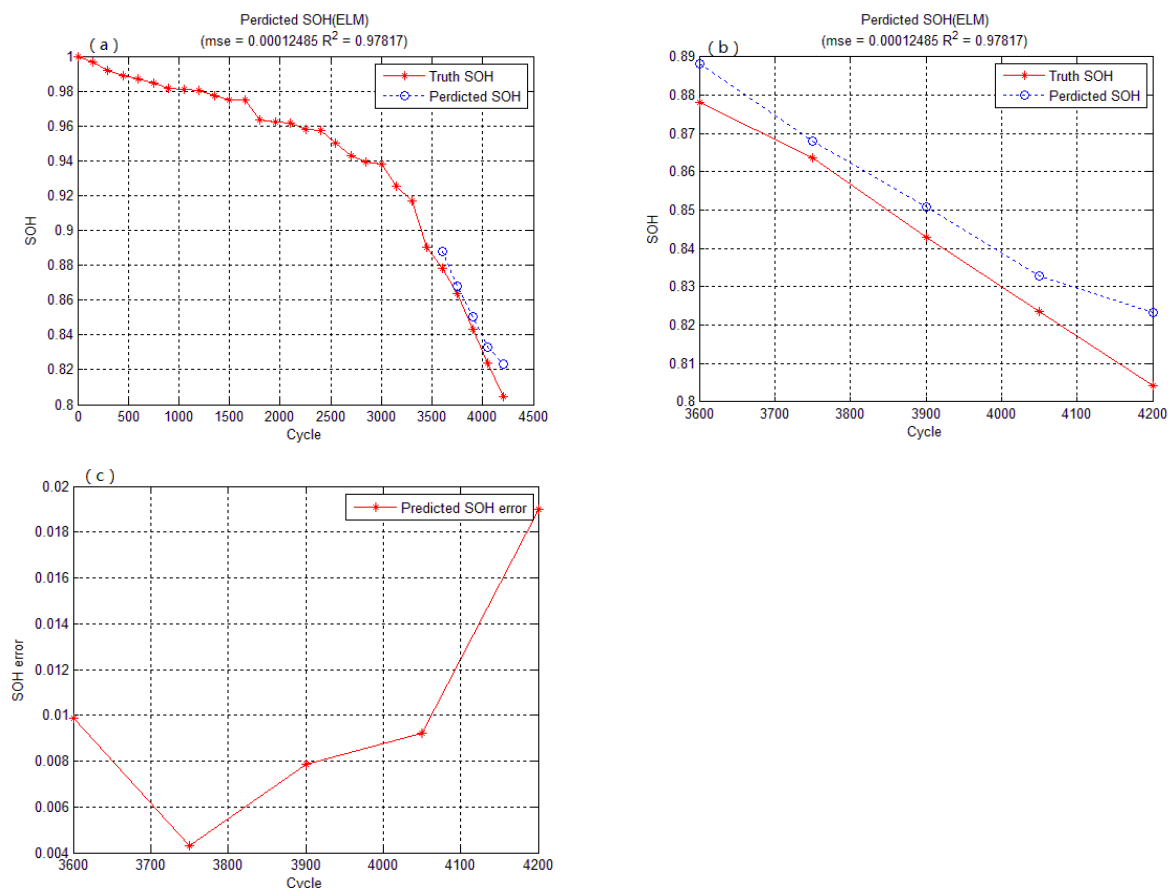


Figure 8. OS-ELM-predicted (a) (b) SOH and (c) error according to the time of equal discharge voltage difference

Sin and hardlim functions were thus tried, and the predicted results and errors are shown in Fig. 7. Compared with those in Fig. 5, all the errors are larger than the error shown in Fig. 5(c).

The predicted discharge time in model 1 is inputted to model 2, and model 2 predicts the battery capacity and calculates the SOH. The predicted results and error are shown in Fig. 8. In Fig.

8(a), the blue hollow circles represent the predicted SOH calculated from Eq. (7). The red asterisks represent the true SOH. The predicted SOH tracks the true SOH variation of the battery well. In Fig. 8(b), the detailed comparison of predicted and true SOH is amplified. In Fig. 8(c), the red asterisks represent the predicted error obtained using the predicted SOH subtracted by the true SOH. All the errors are less than 0.019, which again proves the accuracy of the OS-ELM algorithm.

As discussed in Section 1, many other methods can predict SOH. However, the proposed method is more accurate than other methods. For example, the error of the optimized RVM algorithm when used for RUL prediction is 9% [12]. The error of the EMD–ARIMA method varies from 2.2% to 37% [13] with battery fading. The error of the FFNN–IS method in estimating lithium-ion battery RUL online is 3% to 5% [15]; the neuron number of the hidden layer in FFNN is 50, which increases the computational cost. Compared with the errors of all these methods, the predicted errors based on OS-ELM in this study are smaller.

5. CONCLUSIONS

To solve the problem of directly measuring capacity in prediction of lithium-ion battery SOH, this study used the discharge time of equal voltage interval as the HI and constructed the OS-ELM method for the indirect prediction of lithium-ion battery SOH. The lithium battery fading experiment data were used to verify the OS-ELM algorithm, which was shown to demonstrate good SOH prediction ability. The method has the advantages of convenient data measurement, simple algorithm, high processing speed, and accurate results. Two OS-ELM models were built in this study. Model 1 was used to predict the discharge time of equal voltage interval. Model 2 was used to predict battery SOH according to the predicted discharge time. The predicted error was less than 0.019, which proved the high accuracy of the proposed method. The method was not been tested in a real vehicle. Nevertheless, this study provides a theoretical framework and reference for SOH research on battery management systems.

ACKNOWLEDGMENTS

This work was sponsored by the National Natural Science Foundation of China (Grant No. 51275367).

References

1. Bole B, Kulkarni C, Daigle M, Annual Conference of the Prognostics and Health Management Society, (2014).
2. Liu DT, Pang JY, Zhou JB, Peng Y, IEEE Prognostics & System Health Management Conference, (2012) 1.
3. Zhou JB, Liu DT, Peng Y, Peng XY, IEEE International Instrumentation and Measurement Technology Conference, (2012) 2196.
4. Saha B, Goebel K, *International Journal of Prognostics and Health Management*, 6 (2011) 1.
5. Olivares BE, Munoz MAC, Orchard ME, Marcos E. Orchard, Jorge F. Silva, *IEEE Trans. on Instrumentation and Measurement*, 62 (2013) 364.

6. Jingyue Pang, Yuntong Ma, Datong Liu, Yu Peng, *China Science Paper*, 1 (2014) 28.
7. Yuanyuan Jiang, Zhu Liu, Hui Luo, Hui Wang, *Journal of Electronic Measurement and Instrumentation*, 2 (2016) 179.
8. Kevin L. Gering, *Electrochimica Acta*, 228 (2017) 636.
9. Weijun Gu, Zechang Sun, Xuezhe Wei, Haifeng Dai, *Electrochimica Acta*, 133 (2014) 107.
10. Shrihari Sankarasubramanian, Balaji Krishnamurthy, *Electrochimica Acta*, 70 (2012) 248.
11. Wu H, Yuan S, Zhang X, Yin C, Ma X, *J Power Sources*, 287 (2015) 108.
12. Zhou Y, Huang M, Chen Y, Tao Y, *J Power Sources*, 321 (2016) 1.
13. Zhou Y, Huang M, *Microelectron Reliability*, 65 (2016) 265.
14. Laisuo S, Zhang J, Wang C, Zhang Y, Li Z, Yang S, Jin T, Ma Z, *Applied Energy*, 163 (2016) 201.
15. Wu J, Zhang C, Chen Z, *Applied Energy*, 173 (2016) 134.
16. Wang D, Yang F, Tsui K-L, Zhou Q, Bae SJ, *IEEE Trans Instrument Measurement*, 65 (2016) 1282.
17. Yongshan Zhang, Jia Wu, Chuan Zhou, Zhihua Cai, *Pattern Recognition*, 68(2017) 52.
18. Gao Huang, Guang-Bin Huang, Shiji Song, Keyou You, *Neural Networks*, 61(2015) 32.
19. N.Y. Liang, G.B. Huang, P. Saratchandran, *IEEE Transactions on Neural Networks*, 17 (2006) 1411.
20. J.W. Zhao, Z.H. Wang, D.S. Park, *Neurocomputing*, 87 (2012) 79.
21. USABC electric vehicle Battery Test Procedures Manual, Revision 2, Office of Scientific & Technical Information Technical Reports, (1996), USA.
22. Matthieu Dubarry, Cyril Truchot, Mikaël Cugnet, BorYannLiaw, Kevin Gering, Sergiy Sazhin, David Jamison, Christopher Michelbacher, *J Power Sources*, 196(2011) 10328.
23. Matthieu Dubarry, Cyril Truchot, BorYannLiaw, Kevin Gering, Sergiy Sazhin, David Jamison, Christopher Michelbacher, *J Power Sources*, 196 (2011) 10336.
24. Yang Gao, Caiping Zhang, Qiujiang Liu, Yan Jiang, Weiqiang Ma, Yong Mu, *IEEE Transportation Electrification Asia-Pacific*, (2014) 1.
25. Hongjie Wu, Shifei Yuan, Xi Zhang, Chengliang Yin, Xuerui Ma, *J Power Sources*, 287 (2015) 108.
26. Yiduo Zhu, Fuwu Yan, Jianqiang Kang, Changqing Du, *Ionics* (2017), doi:10.1007/s11581-016-1968-7.